Nuclear Science and Techniques (2026) 37:76
https://doi.org/10.1007/s41365-026-01895-5

Systematic explorations for the effect of nitric acid on radiolysis of TODGA/kerosene: extraction behavior and DFT investigations for the complexation of lanthanides

Jia-Wei Zheng[1] · Shu-Yi Yang[1] · Hao Wu[1] · Yan Wu[1] · Yue-Zhou Wei[1]

Received: 16 November 2024 / Revised: 8 April 2025 / Accepted: 10 April 2025 / Published online: 9 February 2026

Abstract
N,N,N',N'-tetraoctyl diglycolamide (TODGA) is a potential extractant for the co-extraction of lanthanides and actinides in high-level liquid waste. In this study, the radiolysis and extraction properties of TODGA in kerosene solvents contacted with the aqueous phase of varying HNO_3 concentrations were systematically investigated, and the complexation mechanism was analyzed in conjunction with density functional theory (DFT) calculations. After γ-irradiation, the variation of TODGA concentration was detected, and the variation trends in the relative content of radiolysis products (RPs) with sample type and absorbed dose were demonstrated. Results indicated that the breaking of the amide bond, ether bond, and C_{amide}–C_{ether} bond was the primary radiolysis routes. The aqueous-phase precipitate was studied as a potential new mode of TODGA radiolysis in ultrapure water aqueous phase. Moreover, TODGA/kerosene exhibited excellent extraction capabilities for lanthanides even after absorbing 100 kGy, and HNO_3 can maintain a portion of TODGA's extraction capacity. The DFT method was applied to calculate and evaluate the complexing ability of TODGA and some of its RPs toward lanthanides. The results revealed that the complexing ability of TODGA for Ce(III), Eu(III), and Dy(III) was enhanced successively, and the complexing ability of the RPs with intact oxygen-containing structures could not be neglected.

Keywords TODGA · Kerosene · Systematic research · Radiolysis product · Extraction · DFT calculation

1 Introduction

With the development of human society, the demand for nuclear energy is increasing rapidly. High-level liquid waste (HLLW), which is generated from the reprocessing of spent nuclear fuel [1–3], contains a considerable quantity of minor actinides (e.g., Np, Am, and Cm) and other fission products [4–6]. Actinides exhibit exceedingly long half-lives, posing persistent radiological hazards to the environment [7]. Various process flows such as TRPO, DIDPA, TRUEX, and DIAMEX have been proposed for the separation and extraction of actinides from HLLW [8–11]. The nature of HLLW is complex because of its intense radioactivity, high thermal release, and strong acidity [12, 13]. The complexity of HLLW imposes stringent requirements on the separation materials for actinides. In recent years, considerable research has focused on amide ether extractants because of their robust extraction capabilities for actinides and their conformity to the "C, H, O, N" principle [14, 15]. N,N,N',N'-tetraoctyl diglycolamide (TODGA), a notable tridentate ligand extractant (Fig. 1) that enhances metal ion coordination by utilizing a carbonyl group and ether oxygen atoms [16–18], is broadly studied.

TODGA has been extensively explored for many separation processes, including the EURO-GANEX process [19–21] and the i-SANEX process [22–24], and it exhibited great efficacy for the extraction of actinides in acidic environments. Considerable recent research has investigated the radiolysis and extraction properties of TODGA in various organic solvents and ionic liquids [25]. Moreover, during extraction, TODGA could form a third phase

This research was technically supported by Instrumental Analysis Center, Shanghai Jiao Tong University.

✉ Yan Wu
wu_yan@sjtu.edu.cn

[1] Institute of Nuclear Fuel Cycle and Materials, School of Mechanical Engineering, Shanghai Jiao Tong University, Shanghai 200240, China

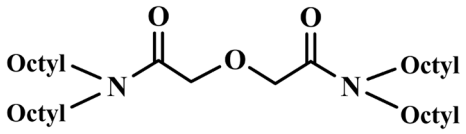

Fig. 1 TODGA structure

because of the splitting of the organic phase [26], which impedes the extraction. TBP, DHOA, octanol, and decanol can mitigate third-phase formation as phase modifiers [27]. Given the high radiation produced by actinides and the other fission products contained in HLLW, the radiolysis of TODGA occurs to some extent with the formation of radiolysis products (RPs), which can detrimentally affect the extraction efficiency of metal ions. The impact of distinct diluent compositions on the radiolysis of TODGA exhibits a diverse range of outcomes. In general, n-dodecane (nDD) is a broadly selected option to dilute TODGA with various phase modifiers [27, 28]. Hydrogenated tetrapropylene [29], iso-paraffins C_{13}–C_{14} [30, 31], and ionic liquids ([C_2mim][NTf_2] [25, 32, 33] and [N_{1888}][NO_3] [34, 35]) are also used as organic solvent for TODGA. During irradiation in these solutions, the extent and form of radiolysis undergone by TODGA are dependent upon the solvent in question. For example, nDD exerts a sensitization effect on the radiolysis of TODGA, as well as phase modifier 1-octanol [36]. However, the radiolysis dose constants of TODGA in [N_{1888}][NO_3] diluent are around four times lower than those in nDD diluent with the same γ energies, dose rates, and absorbed doses [34]. The attack of TODGA by diluent radicals (H·, CH_3·, $CH_3(CH_2)nCH_2$·, etc.) is the most likely radiolysis mechanism, which subsequently results in the breaking of TODGA's bonds. The amide bond, ether bond, and C_{amide}–C_{ether} bond are more inclined to fracture than the other bonds of TODGA, and the cleavage of the octyl side chain is a radiolysis form [16]. The nature of the radicals produced by solvents varies with the specific solvent in use, resulting in the different radiolysis pathways of TODGA.

Apart from the aforementioned solvents, high-purity kerosene is also a viable and cost-effective organic solvent, and it is extensively applied in industrial processes to dilute TODGA. TODGA has been developed for many years as supported by many European Union Framework Programme-funded consortia [37]. In these programs, the TODGA/kerosene system was mostly selected for the extraction of trivalent metal ions from the HNO_3 solution [38]. The i-SANEX process was conducted using TODGA as the extracting species in a kerosene-based diluent with 1-octanol as the phase modifier [39, 40]. The design improvements for the EURO-GANEX process were proposed on the basis of the research of actinide separation using kerosene as the diluent [41, 42]. Moreover, the CHON-UNEX process was designed using TODGA dissolved in kerosene to co-extract trivalent actinides and lanthanides [43]. These studies demonstrate the practicality and cost-effectiveness of kerosene as a diluent for TODGA. In these kerosene-based research systems, the determination of extraction conditions is necessary. However, theoretical data patterns to guide the design and conduct extraction are lacking because of the absence of systematic studies on the radiolysis and extraction properties of TODGA in kerosene systems. Similarly, the generation and semiquantitative analysis of the RPs of TODGA in two phases under kerosene solvents have seldom been studied. Thus, assessing the stability of TODGA under ionizing irradiation conditions and determining the effect of kerosene solvents on TODGA are necessary to facilitate the further application of TODGA/kerosene.

Furthermore, as HNO_3 is an essential part of solvent extractions performed in the reprocessing of spent nuclear fuel, predicting that its effect on the radiolysis of TODGA is crucial [28]. In some previous studies, HNO_3 was shown to be able to facilitate the radiolysis of TODGA as a sensitizer [44, 45]. On the contrary, HNO_3 seemed to have no evident effect [16], or it showed a protective effect [29]. Therefore, conducting a systematic and comprehensive investigation into the radiolysis and extraction properties of TODGA is of great importance when utilizing kerosene as a diluent with aqueous-phase HNO_3. In addition, elucidating the relationship between the concentration of HNO_3 and the radiolysis of TODGA in kerosene solvents is crucial, a topic that has not been extensively explored.

Moreover, TODGA can co-extract some fission products, including Ni, Sr, Zr, Ru, Mo, and Pd, with lanthanides and actinides [37]. Considering the chemical similarity between trivalent lanthanides and minor actinides, the lanthanides Ce(III), Eu(III), and Dy(III) were selected as representative extraction targets, encompassing light, medium, and heavy elements of the lanthanides, to assess the extraction performance of TODGA/kerosene.

Therefore, this study aimed to explore the impact of HNO_3 concentration and absorbed dose on the radiolysis performance of the TODGA/kerosene/HNO_3 system and its extraction efficiency for rare-earth elements contained in simulated solution mixed with other fission product elements. In addition, the presence of RPs in the aqueous phase was identified and subjected to semiquantitative analysis, in a manner consistent with that used for the organic phase. During irradiation, the TODGA/kerosene/ultrapure water system yielded some white precipitates, which were subjected to further detection and analysis in this study. Furthermore, variations in the extraction efficacy of TODGA are found among the lanthanides, and then, density functional theory (DFT) calculations were performed to assess the complexing ability of TODGA toward the lanthanides Ce(III), Eu(III), and Dy(III) in a quantitative manner. A

comparison was conducted between the DFT calculations and the experimental results to verify the changes in the affinity of TODGA for lanthanides. This method can also be used to evaluate the extraction performance of TODGA for actinides. Some RPs of TODGA also exhibited a residual extraction capacity that could not be evaluated directly, but it could be calculated using the DFT method to initially determine the difference in extraction performance between the individual RPs and to assess and compare the complexing ability of these RPs for the same extraction target.

2 Experimental

2.1 Reagents

TODGA (≥ 90%) was synthesized in our laboratory in accordance with the previous literature [46]. Low-odor kerosene was purchased from Alfa Aesar A Johnson Matthey Company. $Ni(NO_3)_2{\cdot}6H_2O$, $Sr(NO_3)_2$, $Ce(NO_3)_3{\cdot}6H_2O$, $Eu(NO_3)_3{\cdot}6H_2O$, and $Dy(NO_3)_3{\cdot}5H_2O$ were all obtained from Sinopharm Chemical Reagent Co., Ltd. Unless otherwise stated, all chemicals were analytically pure and were not further purified.

2.2 Solution preparation

TODGA was diluted to 0.05 mol/L using kerosene for irradiation and extraction test. The prepared TODGA/kerosene solution was injected into the glass headspace vial and then contacted with various HNO_3 concentrations. The organic and aqueous phases were 2 mL in volume. The specific sample information is shown in Table 1.

2.3 Gamma irradiation

All samples were irradiated by a ^{60}Co-γ source ($3.7{\times}10^{15}$ Bq, Shanghai Institute of Applied Physics, Chinese Academy of Sciences) in the air at room temperature (25 ± 5 °C). The absorbed dose ranged from 10 to 1000 kGy with a dose rate of 5.8 kGy/h, as determined by a Fricke dosimeter.

Table 1 Irradiation samples of TODGA under various conditions

Sample	Organic phase	Aqueous phase	Absorbed dose
T1		/	
T2		Ultrapure water	
T3	TODGA/kerosene	0.5 mol/L HNO_3	10–1000 kGy
T4		3.0 mol/L HNO_3	
T5		4.0 mol/L HNO_3	

2.4 UPLC–QTOF–MS measurements

Ultra-high-performance liquid chromatography (UPLC; Acquity UPC2, Waters, USA) and quadrupole time-of-flight mass spectrometry (QTOF–MS; Xevo G2-XS QTOF, Waters, USA) were utilized to quantify the concentration of TODGA and semiquantitatively analyze the RPs. The organic and aqueous phases were detected. The samples before and after irradiation were diluted by a factor of 1×10^2 (aqueous phase, diluted in ultrapure water) and 1×10^3 (organic phase, diluted in methanol). The specific measurement condition settings are presented in the following paragraph.

UPLC was conducted using an Acquity UPLC BEH C8 liquid chromatography column (1.7 µm, 2.1 mm × 100 mm) at 45 °C to separate components. The organic mobile phase was acetonitrile with formic acid (0.1% v/v), and the aqueous mobile phase was ultrapure water with formic acid (0.1% v/v). The mobile-phase flow rate was 0.4 mL/min with a 2 µL injection volume. The mass spectrometer conditions were as follows: desolvation temperature, 450 °C; source temperature, 120 °C; desolvation gas flow, 800 L/h; capillary voltage, 2.0 kV; electrospray ionization source, positive mode; and mass spectrometry scanning range (m/z), 50–2000. The data were processed using the Waters UNIFI Scientific Information System, and the mass target match tolerance was less than 5 ppm.

2.5 Extraction experiments

The extraction solutions comprised Ni(II), Sr(II), Ce(III), Eu(III), and Dy(III) at a concentration of 100 µg/mL in 3.0 mol/L HNO_3. Then, 1 mL organic-phase sample was mixed with the extraction solutions at a phase volume ratio of 1:1 using a vortex mixer (Vortex-2, Shanghai Huxi Industry Co., Ltd., Shanghai) at 25 °C and a speed of 2000 rpm. The concentrations of metal ions were confirmed using the Inductively Coupled Plasma-Atomic Emission Spectroscopy (ICPS-7510, Shimadzu, Japan). Furthermore, a loading test for Ce(III), Eu(III), and Dy(III) by TODGA was performed at concentrations ranging from 100 to 1400 µg/mL.

2.6 DFT calculations

All DFT calculations were carried out using the Gaussian 16 program package [47–49], and the structures were drawn in Gaussian View 6.0 software [50]. The theoretical level of B3LYP/6-31 G(d) was applied to the optimization and frequency calculations of TODGA and its RPs. For the complexation of ligands and the lanthanides (Ce(III),

Eu(III), and Dy(III)), the PBE0 functional can well reflect the interaction of the transition metal complexes [51]. The Ce(III), Eu(III), and Dy(III) atoms were handled using the Stuttgart and Dresden quasi-relativistic effective core potentials ECP47MWB, ECP52MWB, and ECP55MWB, respectively, considering the relativistic effects of the lanthanides. Moreover, the 6-31 G(d) basis set was applied to the light atoms C, N, O, and H. Therefore, the optimization and frequency calculations of complexation were performed at the theoretical level of PBE0/6-31 G(d)/RECP, considering the DFT-D3(BJ) dispersion corrections.

The optimization and frequency calculations of trivalent lanthanide complexes with TODGA or TODGA's RPs ligands were particularly time-consuming [52]. Therefore, we used tetramethyl diglycolamide (TMDGA) to replace TODGA; that is, the octyl structures of TODGA and its RPs were substituted with methyl. In accordance with previous research, the stoichiometric ratio of the ligands and trivalent lanthanides was predominantly 3:1 [28], and the nitrates were also considered. The binding energy (E), Gibbs free energy (G), and enthalpy (H) were calculated under gas-phase conditions at 298.15 K with the same theoretical level. The Ln(III)–O bond length of complexes, the highest occupied molecular orbital (HOMO), and the lowest unoccupied molecular orbital (LUMO) of TODGA and RPs were analyzed on the basis of the optimized structures and frequency calculation results. In addition, the electrostatic potential mapping (ESP) of TODGA and RP analyses were performed using the Multiwfn (version 3.8(dev)) wavefunction processor [53–55], and the results of ESP mapping were visualized by using Visual Molecular Dynamics (VMD 1.9.3) package [56].

3 Results and discussion

3.1 Quantitative analysis of TODGA

The concentrations and radiolytic stability of TODGA were detected and evaluated by using UPLC–QTOF–MS. As shown in Fig. 2, the concentrations of TODGA varied with the type of aqueous phase and absorbed dose. The decrease in TODGA concentration was not severe as doses of up to 100 kGy were absorbed. However, the concentrations of TODGA differed significantly among samples, and they were higher in the presence of HNO_3 at the absorbed dose of 500 and 1000 kGy, indicating that HNO_3 can protect TODGA against the γ-radiolysis. In addition, the protective effect was stronger at a higher HNO_3 concentration. Moreover, ultrapure water accelerated the radiolysis of TODGA compared with the other samples, reaching a radiolysis degree of approximately 80% at 1000 kGy.

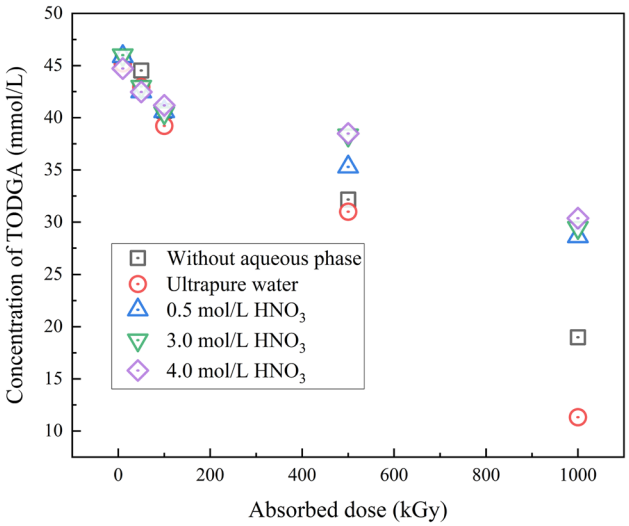

Fig. 2 (Color online) Concentrations of TODGA under various conditions

Apart from the direct radiolysis of TODGA by γ-irradiation, which also results in the formation of radicals and RPs of the kerosene diluent, the radiolysis of alkanes in kerosene is represented by Eq. (1) [57].

$$\begin{aligned} &CH_3(CH_2)nCH_3 \rightsquigarrow \gamma \rightsquigarrow CH_3(CH_2)nCH_3\cdot^+ \\ &\quad +CH_3(CH_2)nCH_3\cdot + \cdot CH_3 + H\cdot + H_2 \end{aligned} \tag{1}$$

The radicals have active redox properties, and they directly attack the structure of TODGA by transferring electrons or positron holes. However, numerous radicals and certain RPs of HNO_3, including HNO_2, NO_2^-, $\cdot NO_3$, $H\cdot$, and $\cdot OH$, are produced in the aqueous phase. These species engage in reactions with the radicals generated from the kerosene diluent, thereby diminishing the interactions between the radicals and TODGA. Consequently, the radiolysis of TODGA is inhibited, illustrating the protective effect exerted by HNO_3.

In this study, the radiation-chemical yields (G_r) of TODGA in all samples at the absorbed doses of 10–1000 kGy were determined, and the results are presented in Table S1. Results demonstrated a gradual decrease in G_r of TODGA with the increase in absorbed dose under the same aqueous-phase conditions. Furthermore, the G_r values of the TODGA systems under nitric acid conditions were approximately 27.0 nmol/J at 500 kGy and 24.5 nmol/J at 1000 kGy, which were about 40% lower than those of the systems without nitric acid at the same absorbed doses, indicating the protective effect of nitric acid at a high absorbed dose. In addition, the G_r values of TODGA in kerosene solvent are approximately an order of magnitude lower than those observed in nDD solvent, as reported in previous studies [28, 58].

To investigate the effects of organic solvent and absorbed dose on the radiolysis of TODGA, comparative analysis is presented in Table S2. This analysis indicates that the presence of kerosene may slow down the radiolysis of TODGA compared with that observed for nDD and ionic liquid $[N_{1888}][NO_3]$. Kerosene, comprising a combination of various alkanes, generates free radicals in a more intricate and varied manner than nDD and ionic liquids. The reactivity of these free radicals may facilitate interactions among them, thereby reducing the direct attacks on the TODGA structure. Consequently, the radiolysis degree of TODGA is diminished in comparison with other systems. The use of kerosene solvents may contribute to a stable extraction environment for TODGA, enhance its utilization, and lower the costs associated with industrial applications.

3.2 Semiquantitative analyses of RPs

By using high-resolution MS and analyzing its detection results, Table S3 shows 18 potential RPs of TODGA and their molecular formula and neutral mass information. Semiquantitative data were obtained from the chromatographic peak areas of $[M+H^+]$ (M is the detected compound, and H^+ is the adduct) ions, representing the relative concentration of RPs. The ionization potential of different molecules varies, resulting in different ionization efficiencies, which leads to semiquantitative results. In addition, the results of the peak area data are shown in Fig. 3 with normalized detector counts, as a function of the absorbed dose and the type of aqueous phase. This result indicates whether the molecules were already present in the unirradiated samples or were formed because of γ-irradiation. The intensities of the $[RP8+H^+]$ and $[RP13+H^+]$ peaks were lower than the noise threshold; therefore, RP8 and RP13 are not visible in Fig. 3. Some RPs were detected in the unirradiated samples, such as RP1, RP4, RP7, RP9, RP12, and RP18. Dioctylamine is the raw material for the synthesis of TODGA [59]; thus, RP1 also existed as an impurity in TODGA solutions before irradiation. RP7 might be formed by RP1 oxidation. After absorbing a low dose of γ-irradiation (less than 100 kGy), the $[M+H^+]$ peak areas of RP4, RP9, and RP12 increased. Therefore, these three RPs were present in small amounts as by-products during the synthesis of TODGA, but more of them were produced because of γ-irradiation [60].

The dominant variation trends in the relative contents of RPs initially increased and then decreased with the increase in absorbed dose. The turnaround in trends mainly occurred at the absorbed doses of 100 or 500 kGy. The contents of the RPs increased with the aggravation of TODGA radiolysis and decreased as a consequence of self-radiolysis. However, the contents of RP3, RP5, RP10, and RP15 mainly showed a continuously increasing trend with the increase in the absorbed dose. Furthermore, the production of different RPs and their relative content were affected in varying ways by the presence or absence of HNO_3 and the HNO_3 concentration in the aqueous phase. For example, the variation trend of RP12 was dramatically altered by high concentration (3.0 and 4.0 mol/L) of HNO_3.

The contents of RP4, RP16, RP17, and RP18 were relatively higher in the presence of HNO_3 as subjected to a high absorbed dose (> 200 kGy), whereas RP11 and RP14 exhibited a relatively lower concentration. The structures of RP4, RP16, and RP17 are similar to the structure of TODGA, and the distinctions occur in the octyl moiety chain. The formation of RP16 is related to the oxidation effect of HNO_3 or its RPs on the C–C bond in octyl near the N atom. In addition, the formation of RP17 is probably due to the interaction between the C atom in the C_{octyl}–N bond and NO_3^-. The low contents of RP11 and RP14 in the presence of HNO_3 demonstrate that the cleavage of the C_{amide}–C_{ether} bond and C–O ether bond is inhibited by HNO_3. Moreover, RP11 would be oxidized to RP18 by HNO_3 or its RPs, similar to the formation of RP16. Thus, the content of RP18 was higher with HNO_3, whereas the content of RP11 was lower.

The contents of RP1, RP3, RP7, RP9, RP10, and RP15 were relatively lower in the presence of high HNO_3 concentrations as subjected to a high absorbed dose, whereas RP5, RP6, and RP17 exhibited a relatively higher concentration. RP1, RP3, and RP10 were generated from the breaking of the amide bond, ether bond, and C_{amide}–C_{ether} bond, respectively. Then, the oxidation of octyl in RP1 and the breaking of the C_{octyl}–N bond in RP3 and RP10 separately lead to the formation of RP7, RP15, and RP9.

Based on the above-mentioned results and analysis, the prime radiolysis pathways of TODGA are the rupture of the amide bond, ether bond, C_{amide}–C_{ether} bond, and C_{octyl}–N bond, whereas the breaking of these bonds is inhibited by the high concentration of HNO_3. However, the octyl structure of TODGA would be oxidized by HNO_3, a different degradation pathway. Meanwhile, some RPs are subjected to further radiolysis, and they undergo structural alterations, resulting in the formation of novel RPs.

Four RPs (RP5, RP7, RP9, and PR15) were identified and semiquantitatively analyzed in the aqueous phase, and the results of the peak area data are shown in Fig. 3q–t. The content variations of RP5, RP7, and RP9 were evident in the presence of a high concentration of HNO_3, which increased in the range of 0–50 kGy and decreased within 50–100 kGy under 4.0 mol/L HNO_3. However, the content of RP15 was higher in the sample of ultrapure water and 0.5 mol/L HNO_3, indicating that the creation of RP15 was inhibited by the high concentration of HNO_3. This finding is attributed to the fact that the lipophilic and hydrophilic properties of diglycolamide compounds can be altered by the attachment of different alkyl side chains to N atoms [61]. For example,

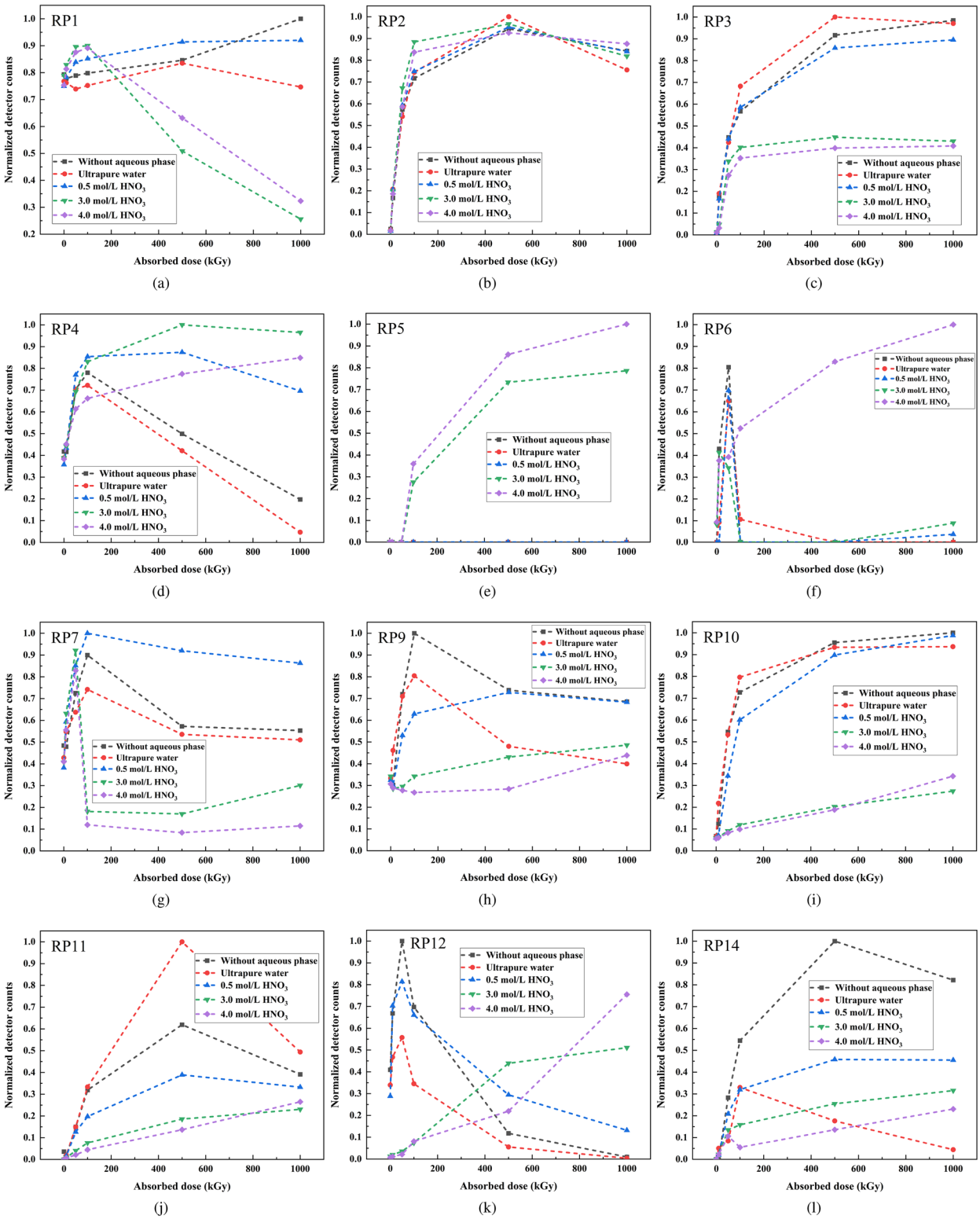

Fig. 3 (Color online) Results of semiquantitative analyses of radiolysis products of TODGA in organic and aqueous phases. **a** RP1, organic phase; **b** RP2, organic phase; **c** RP3, organic phase; **d** RP4, organic phase; **e** RP5, organic phase; **f** RP6, organic phase; **g** RP7, organic phase; **h** RP9, organic phase; **i** RP10, organic phase; **j** RP11, organic phase; **k** RP12, organic phase; **l** RP14, organic phase; **m** RP15, organic phase; **n** RP16, organic phase; **o** RP17, organic phase; **p** RP18, organic phase; **q** RP5, aqueous phase; **r** RP7, aqueous phase; **s** RP9, aqueous phase; and **t** RP15, aqueous phase

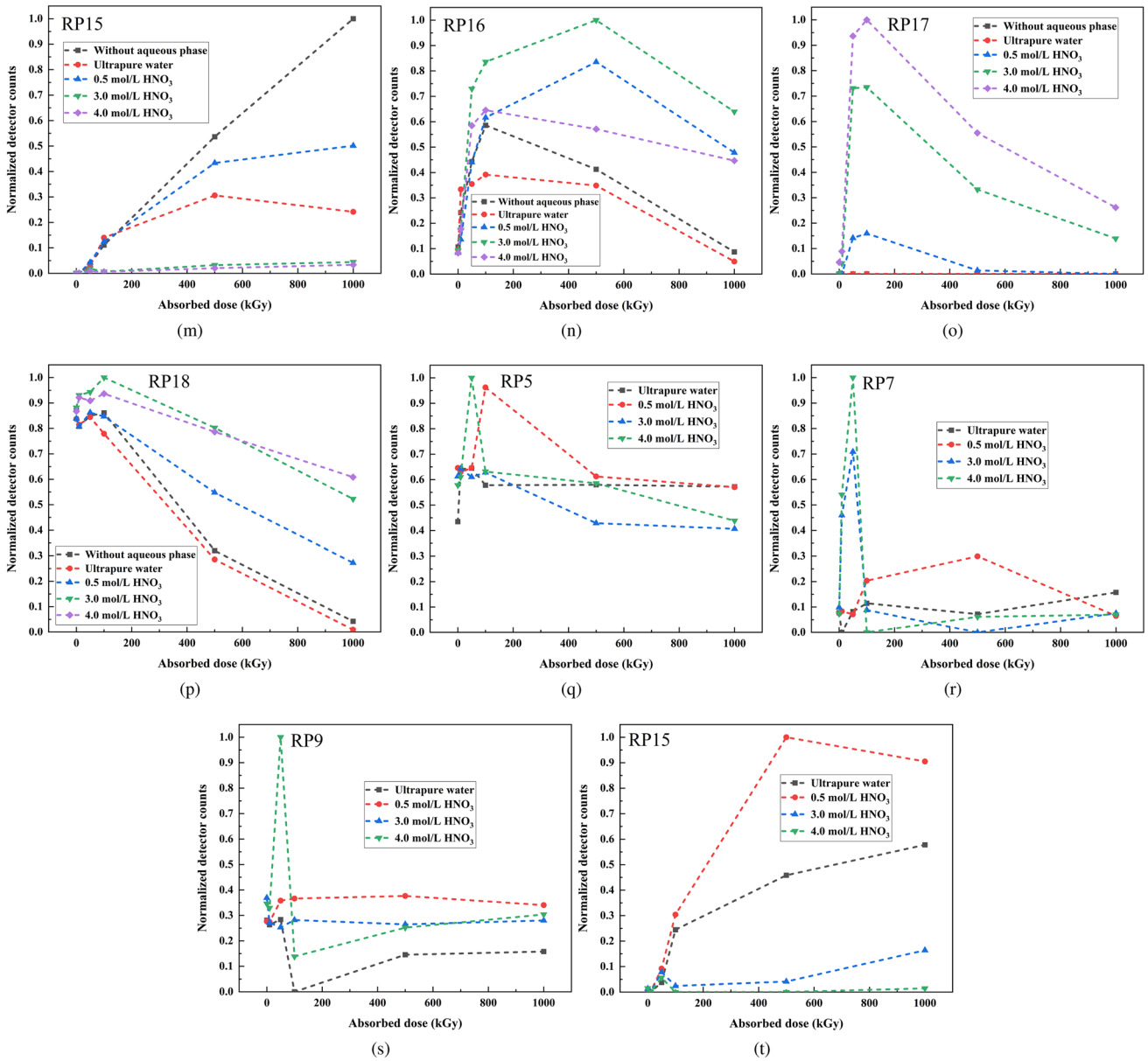

Fig. 3 (continued)

TMDGA, tetraethyl diglycolamide, and tetrapropyl diglycolamide are water-soluble ligands, exhibiting high hydrophilicity with short alkyl chains and lower C/O ratios in their structures than TODGA. In our study, by detecting these four RPs in the aqueous phase, the breaking of the octyl group and the attachment of O atom in the structure of TODGA and its RPs reduce the hydrophobicity of these four RPs with relatively low C/O ratios. Consequently, the four RPs were detected in the aqueous phase in minute quantities.

Based on the identified RPs of TODGA, the radiolysis routes of TODGA in kerosene solvent are illustrated in Fig. 4. As TODGA has a symmetric structure, the five radiolysis routes labeled in the figure also occur at their symmetric sites. The route (e) represents the chemical reactions occurring on the octyl moiety.

There is another noteworthy phenomenon that deserves to be discussed. As shown in Fig. 5, a part of white precipitates was observed at the system of TODGA/ultrapure water in aqueous phase after irradiation. The white precipitate became more pronounced as the absorbed dose increased, and the aqueous phase became saturated with the precipitate as the absorbed dose exceeded 50 kGy. Following the separation of the two phases, the aqueous phase containing the precipitate was subjected to centrifugation to obtain a faint yellow solid powder. Afterward, the powder was redissolved and detected by

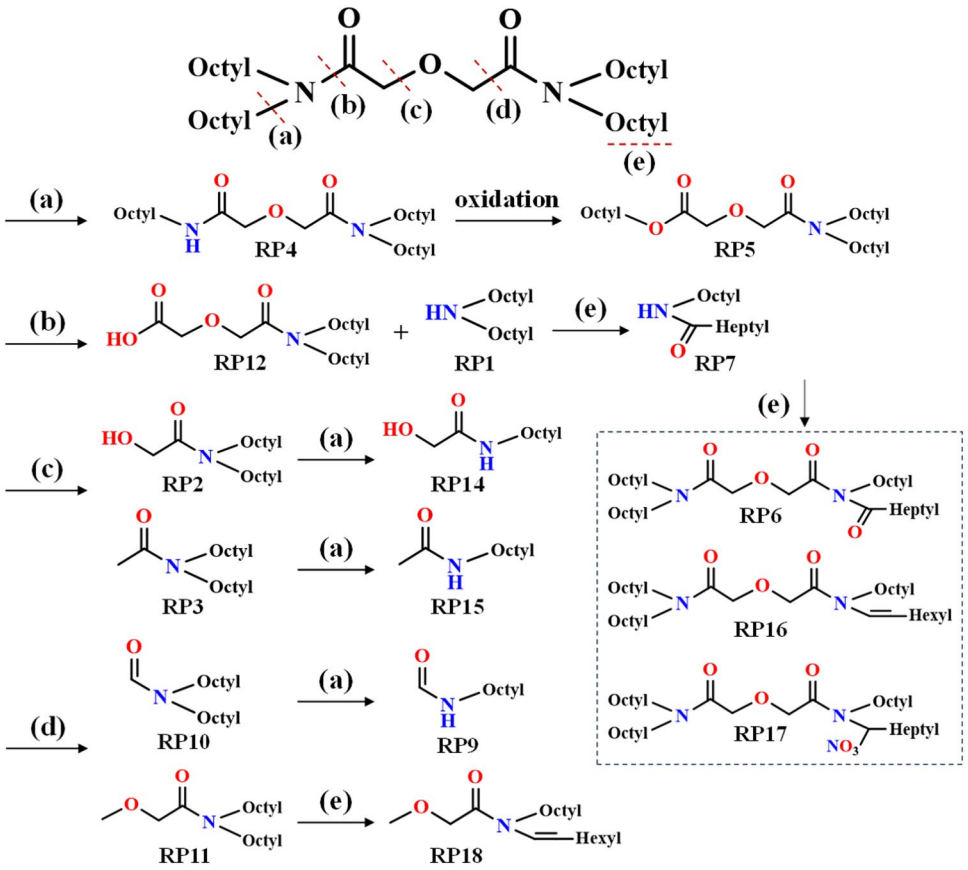

Fig. 4 (Color online) The possible radiolysis routes of TODGA in kerosene contacted with nitric acid solution

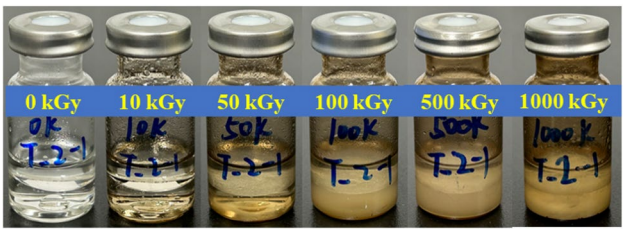

Fig. 5 (Color online) Precipitate in the ultrapure water aqueous phase under various absorbed doses

UPLC-QTOF-MS and the mass-to-charge ratio result was identical to that of TODGA, indicating that TODGA was likely the primary component of the precipitate. The above-mentioned findings indicated that the radicals generated in the aqueous phase may have interacted with the kerosene solvent and TODGA, resulting in the precipitation of TODGA. However, in the presence of HNO_3, the precipitate might be inhibited by the radicals generated from HNO_3 or dissolved by H^+. The precise cause of the precipitate formation remains to be elucidated and requires further investigation. This phenomenon explains why the radiolysis degree of TODGA is highest in ultrapure water samples at a high absorbed dose. Therefore, in the event of high-radiation fields and doses, the impact of precipitation on the efficacy and security of the extraction can be avoided under acidic aqueous-phase conditions.

3.3 Effects of gamma irradiation on extraction experiments

The organic phases of samples T1–T4 before and after irradiation were applied to extract Ni(II), Sr(II), Ce(III), Eu(III), and Dy(III) from 3.0 mol/L HNO_3 solution to evaluate the effects of γ-irradiation on the extraction properties of TODGA. The extraction rates of these metal ions were calculated, and the results are shown in Fig. 6. TODGA exhibited a low extraction capacity for Ni(II) at any absorbed dose and for all sample types. The extraction rates of Sr(II) decreased from approximately 30% to less than 5% as the absorbed dose increased. However, TODGA exhibited a high extraction capacity for Ce(III), Eu(III), and Dy(III), with extraction rates of approximately 100% observed in all samples within the absorbed dose of 100 kGy. Then, a notable decline in the extraction rates of Ce(III), Eu(III), and Dy(III) was observed as the absorbed dose reached 1000 kGy, and

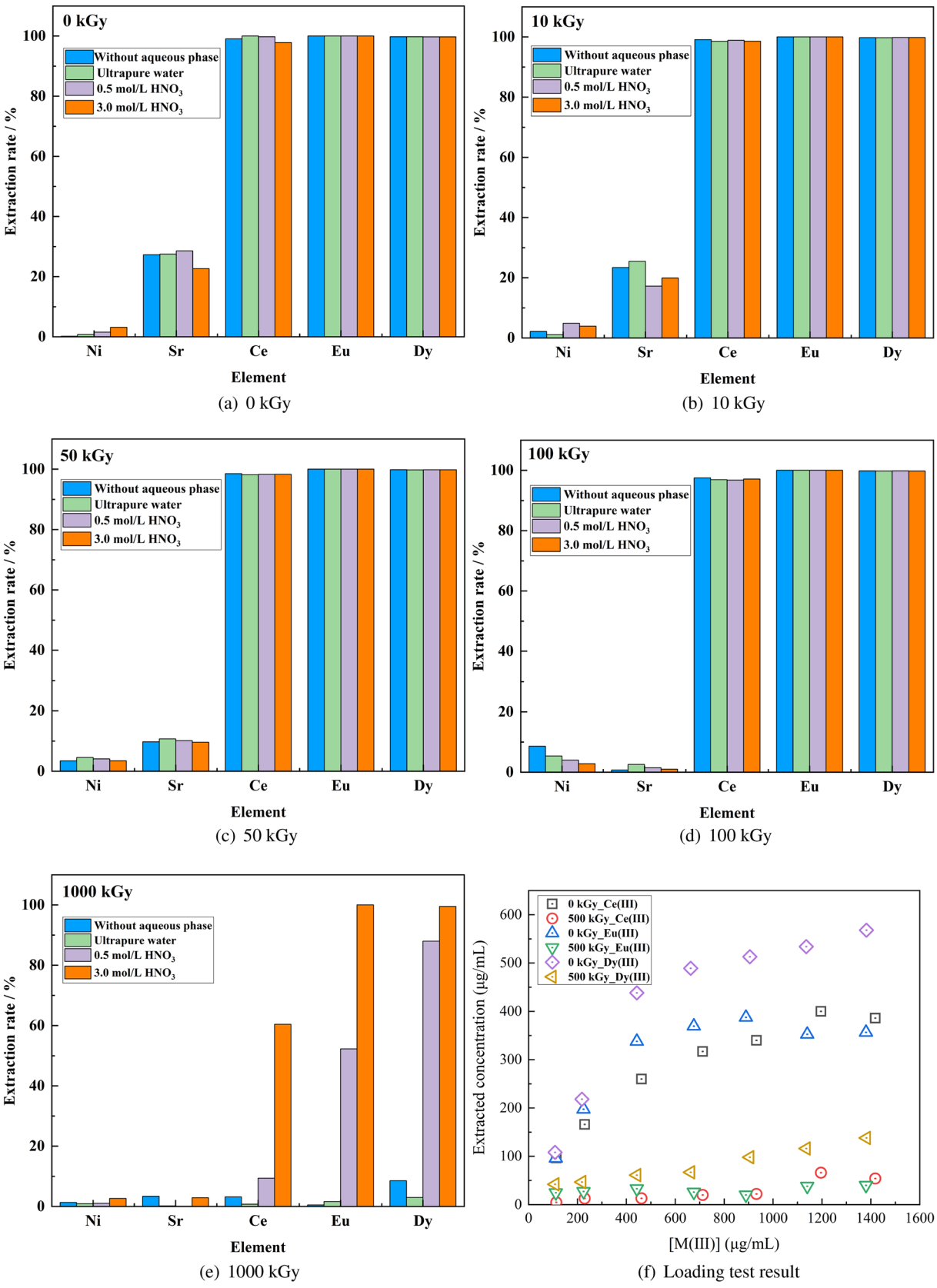

Fig. 6 (Color online) Extraction results of Ni(II), Sr(II), Ce(III), Eu(III), and Dy(III) under various conditions

the four types of samples exhibited discernible differences. The extraction ability of TODGA was partially maintained as the concentration of HNO_3 increased. In addition, the results demonstrated that TODGA exhibited a higher affinity for Eu(III) and Dy(III) than Ce(III).

Loading test investigations were conducted with sample T1 (without aqueous phase) at an absorbed dose of 500 kGy. As illustrated in Fig. 6f, with the increase in Ce(III), Eu(III), and Dy(III) concentrations, the extracted concentrations exhibited a gradual increase and reached equilibrium. The maximum extracted concentrations of Ce(III) and Eu(III) were approximately 350 μg/mL, exhibiting a reduction of approximately 88% after absorbing 500 kGy of γ-irradiation. The maximum extracted concentration of Dy(III) was approximately 550 μg/mL, and a reduction of approximately 75% was observed after irradiation. In addition, TODGA demonstrated a higher capacity for Dy(III) than Ce(III) and Eu(III).

3.4 UPLC-QTOF-MS results of TODGA complexes with Eu(III)

Following the complexation of Eu(III) in extraction experiments without irradiation, the organic phase was separated, and the complexation form of TODGA with Eu(III) was detected using UPLC–QTOF–MS. The MS results are presented in Fig. S1. The ions observed at m/z = 1438.0 and 2018.5 were assigned to $[Eu(TODGA)_2(NO_3)_2]^+$ and $[Eu(TODGA)_3(NO_3)_2]^+$, respectively, and they correspond to complexes formed between TODGA and Eu(III). These ions were consistent with the Eu:TODGA stoichiometries reported in the previous work [62–64], indicating the presence of two types of Eu:TODGA complexes with 1:2 or 1:3. Based on these results, the complexation of TODGA with trivalent lanthanides was studied using DFT theoretical calculations.

3.5 DFT calculations of the complexation of TODGA and RPs with trivalent lanthanides

To further investigate and verify the extraction ability of TODGA and its RPs, the structural properties and complexation reactions of TODGA and RPs with Ce(III), Eu(III), and Dy(III) were studied by DFT calculations. Table S4 presents the changes in binding energy (ΔE), Gibbs free energy (ΔG), and enthalpy (ΔH) for the complexation reactions of TMDGA with Ce(III), Eu(III), and Dy(III), and nitrates were considered in the reactions. The results indicate that all ΔH values are negative, illustrating that the three complexation processes are exothermic and could occur spontaneously. The complexing ability of TODGA toward Ce(III), Eu(III), and Dy(III) is notable, and nitrates play a role in this process. Furthermore, ΔG can be used as an indicator of the likelihood of a chemical reaction occurring and the stability of products formed during chemical reactions. The more negative the value of ΔG, the higher the likelihood of spontaneous product formation from reactants. This results from the release of chemical reaction energy or the increase in entropy of the system as the reaction progresses. Consequently, the reaction rate is typically faster, and the reactants are readily converted into stable products [65, 66]. In this study, the complexing ability of TODGA toward Ce(III), Eu(III), and Dy(III) was enhanced sequentially, as indicated by the decrease in ΔG of the complexation reactions that yielded the complexes $Ce(TMDGA)_3(NO_3)_3$, $Eu(TMDGA)_3(NO_3)_3$, and $Dy(TMDGA)_3(NO_3)_3$, respectively. In addition, the loading test results demonstrated that the loading capacities of TODGA for Ce(III), Eu(III), and Dy(III) increased gradually, which was consistent with the variation trend of the ΔG values.

The complexing abilities of TODGA toward trivalent lanthanides are also reflected by the changes in the Ln(III)–O bond lengths (Table S5). The average Ln(III)–O bond lengths follow the order of Ce(III)–O > Eu(III)–O > Dy(III)–O, indicating that the affinity of TODGA for Ce(III), Eu(III), and Dy(III) increases sequentially, which is consistent with the variation trends of the thermodynamic quantities.

The O atom of the ether bond and carbonyl of ligand plays a dominant role in the complexation reaction [16]. The ether bond and carbonyl groups of RP4, RP5, RP6, RP12, RP16, and RP17 were well preserved among various types of TODGA RPs. Therefore, these six RPs were analyzed theoretically to evaluate their complexing ability.

The HOMO–LUMO gaps of TODGA, RP4, RP5, RP6, RP12, RP16, and RP17 were calculated, and the results are presented in Table 2. In general, the HOMO–LUMO gap is considered as a marker that reflects chemical reactivity and kinetic stability to a certain extent [67], and the molecule is more readily excited as the band gap is narrower. The HOMO–LUMO gaps for these seven structures follow the order of RP17 < RP6 < RP16 < RP12 < RP5 < TODGA <

Table 2 HOMO, LUMO, and HOMO-LUMO energy gaps of TODGA and six radiolysis products (unit: eV)

Type	HOMO	LUMO	HOMO–LUMO gap
TODGA	−6.065	1.000	7.065
RP4	−6.120	1.003	7.123
RP5	−6.148	0.596	6.744
RP6	−6.024	−0.877	5.147
RP12	−6.314	0.266	6.580
RP16	−5.987	−0.316	5.671
RP17	−5.903	−2.302	3.601

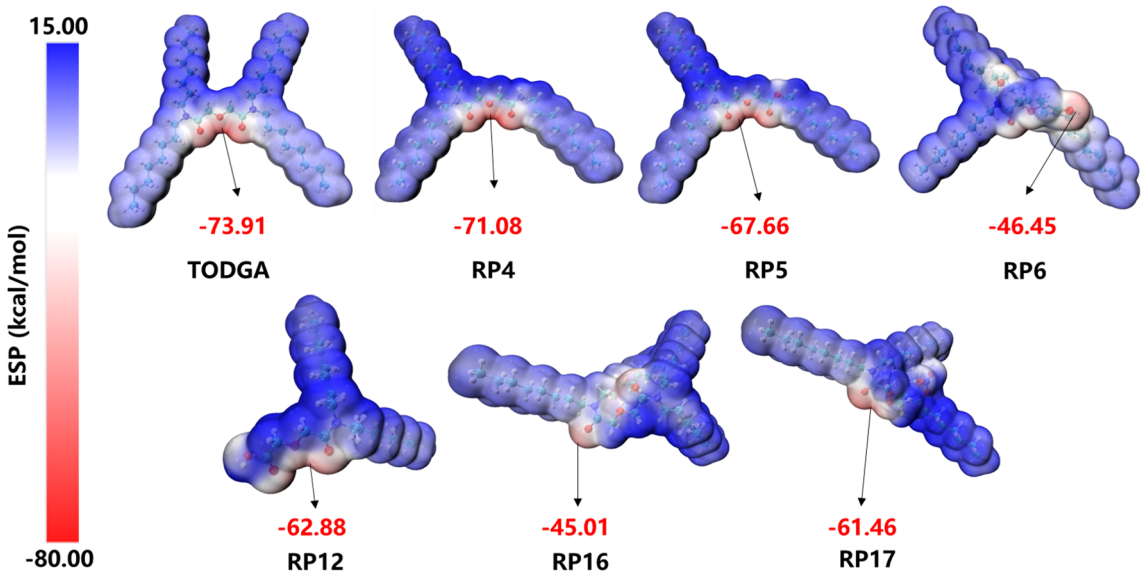

Fig. 7 (Color online) Diagrams of the ESP of TODGA and six radiolysis products at the theoretical level of B3LYP/6-31 G(d). The value (kcal/mol) is the most negative ESP for each structure

RP4. The gaps of RP6, RP16, and RP17 are significantly smaller than those of TODGA, indicating that the structural alteration may result in these three RPs becoming more unstable than TODGA.

The electronic structures of TODGA and six RPs were explored. The electrostatic potential (ESP) diagrams shown in Fig. 7 could be utilized to assess the complexing capacity of extractants and metal ions [68]. The blue and red regions illustrate a positive and negative ESP, respectively. The negative ESP is distributed around the O atoms of the carbonyl groups and ether bond, indicating that these O atoms serve as the preferred binding sites for metal ions. The most negative ESP values of TODGA and six RPs are presented in Fig. 7, following the order of TODGA < RP4 < RP5 < RP12 < RP17 < RP6 < RP16, which indicate that these structures can complex with metal ions. The ESP values of RP4, RP5, and RP12 are more negative than those of RP6, RP16, and RP17, suggesting that RP4, RP5, and RP12 may have a stronger affinity for metal ions. The reaction that occurred in the octyl side chain of RP6, RP16, and RP17 alter the spatial molecular structure of TODGA, which may have an impact on the ESP distribution of TODGA, thereby inhibiting the electron-donating ability of the O atoms in carbonyl groups and the ether bond as the most negative ESP values increase.

Based on the ESP values of the six RPs, RP4, RP5, and RP12 were selected as a substitute to one TMDGA in the structure of $Eu(TMDGA)_3(NO_3)_3$ to explore and compare the complexing ability of the RPs. Thus, theoretical calculations were performed for the complex species $Eu(TMDGA)_2(RP4)(NO_3)_3$, $Eu(TMDGA)_2(RP5)(NO_3)_3$, and $Eu(TMDGA)_2(RP12)(NO_3)_3$. The values of ΔE, ΔG, and ΔH of the complexation reactions (Table S6) and the Eu(III)–O bond lengths of the complexes (Table S7) are presented. The ΔE, ΔG, and ΔH values, as well as Eu(III)–O bond lengths, decrease gradually as the complexes contain RP4, RP5, and RP12. This result demonstrates that RP12 may have greater complexing ability compared with RP4 and RP5 in complexation with trivalent lanthanides. Therefore, the substitution of the octyl side chain with a hydroxyl group in the TODGA structure may preserve the enhanced complexing ability of the ligand, which is superior to that of the other RPs.

4 Summary

γ-Radiolysis of TODGA/kerosene/HNO_3 or ultrapure water and TODGA/kerosene was investigated by analyzing the changes in TODGA concentration and its liquid RPs. Sixteen RPs of TODGA in kerosene and four RPs in aqueous phase were identified and semiquantitatively analyzed using UPLC-QTOF-MS, and the change patterns of their relative contents in every sample were presented. In addition, five radiolysis routes for TODGA were proposed. A comprehensive investigation was conducted into the radiolysis pathways and semiquantitative analysis of RPs of TODGA/kerosene in contact with nitric acid. The results elucidated the preferential reaction sites within the TODGA structure for radical interactions and further illustrated the relationship among these reaction sites, the absorbed dose, and the acidity of the aqueous phase. Thus, additional protective measures can be explored and provided to effectively inhibit the radiolysis

of TODGA/kerosene during extraction. Moreover, the white precipitate was observed in the TODGA/kerosene/ultrapure water system, which could be another form of TODGA radiolysis. TODGA demonstrated higher affinity and loading capacity for Ce(III), Eu(III), and Dy(III) than Ni(II), Sr(II), and it exhibited good resistance to γ-irradiation within 100 kGy. Furthermore, DFT calculations demonstrated that the complexing ability of TODGA toward Ce(III), Eu(III), and Dy(III) was enhanced sequentially, and the RPs of TODGA with a well-preserved ether bond and carbonyl groups possessed good complexing ability with trivalent lanthanides. This study provides further insights into the radiolysis of TODGA under kerosene solvent for the advancement of industrial processes and for the extraction of trivalent actinides and lanthanides.

Supplementary Information The online version contains supplementary material available at https://doi.org/10.1007/s41365-026-01895-5.

Author contributions All authors contributed to the study conception and design. Material preparation, data collection, and analysis were performed by Jia-Wei Zheng, Shu-Yi Yang, and Hao Wu. The first draft of the manuscript was written by Jia-Wei Zheng, and all authors commented on previous versions of the manuscript. All authors read and approved the final manuscript.

Data availability The data that support the findings of this study are openly available in Science Data Bank at https://cstr.cn/31253.11.sciencedb.j00186.00947 and https://www.doi.org/10.57760/sciencedb.j00186.00947.

Declarations

Conflict of interest The authors declare that they have no conflict of interest.

References

1. M. Wei, D. Qiao, J. Chen et al., Study on the benefit of HLLW partitioning on the high-level waste glasses from the viewpoint of waste management. Prog. Nucl. Energy **160**, 104672 (2023). https://doi.org/10.1016/j.pnucene.2023.104672
2. J. Wang, S. Jing, J. Chen, Demonstration of a crown ether process for partitioning strontium from high level liquid waste (HLLW). Radiochim. Acta **104**, 107–115 (2016). https://doi.org/10.1515/ract-2015-2454
3. Y. Wei, X. Wang, R. Liu et al., An advanced partitioning process for key elements separation from high level liquid waste. Sci. China: Chem. **55**, 1726–1731 (2012). https://doi.org/10.1007/s11426-012-4697-4
4. S.C. Zhang, S.Y. Ning, J. Zhou et al., New insight into the adsorption of ruthenium, rhodium, and palladium from nitric acid solution by a silica-polymer adsorbent. Nucl. Sci. Tech. **31**, 34 (2020). https://doi.org/10.1007/s41365-020-0744-6
5. Z.X. Fang, M. Yu, Y.G. Huang et al., Theoretical analysis of long-lived radioactive waste in pressurized water reactor. Nucl. Sci. Tech. **32**, 72 (2021). https://doi.org/10.1007/s41365-021-00911-0
6. B. Liu, J. Han, F. Liu et al., Minor actinide transmutation in the lead-cooled fast reactor. Prog. Nucl. Energy **119**, 103148 (2020). https://doi.org/10.1016/j.pnucene.2019.103148
7. H.Y. Meng, Y.W. Yang, Z.L. Zhao et al., Physical studies of minor actinide transmutation in the accelerator-driven subcritical system. Nucl. Sci. Tech. **30**, 91 (2019). https://doi.org/10.1007/s41365-019-0623-1
8. J.H. Ye, T. Yu, Efficient and selective extraction of uranium from seawater based on a novel pulsed liquid chromatography radionuclide separation method. Nucl. Sci. Tech. **34**, 19 (2023). https://doi.org/10.1007/s41365-023-01180-9
9. H.L. Chen, J.C. Wang, W.H. Duan et al., Hydrodynamic characteristics of 30% TBP/kerosene-HNO_3 solution system in an annular centrifugal contactor. Nucl. Sci. Tech. **30**, 89 (2019). https://doi.org/10.1007/s41365-019-0615-1
10. M.Y. Alyapyshev, V.A. Babain, Y.A. Ustynyuk, Recovery of minor actinides from high-level wastes: modern trends. Russ. Chem. Rev. **85**, 943–961 (2016). https://doi.org/10.1070/RCR4589
11. J.N. Mathur, M.S. Murali, K.L. Nash, Actinide partitioning-a review. Solv. Extr. Ion Exch. **19**, 357–390 (2001). https://doi.org/10.1081/sei-100103276
12. Y. Wu, X. Zhang, S.Y. Kim et al., Simultaneous separation and recovery of Cs(I) and Sr(II) using a hybrid macrocyclic compounds loaded adsorbent. Kinetic, equilibrium and dynamic adsorption studies. J. Nucl. Sci. Technol. **53**, 1968–1977 (2016). https://doi.org/10.1080/00223131.2016.1175979
13. Y. Wu, C.P. Lee, H. Mimura et al., Stable solidification of silica-based ammonium molybdophosphate by allophane: application to treatment of radioactive cesium in secondary solid wastes generated from fukushima. J. Hazard. Mater. **341**, 46–54 (2018). https://doi.org/10.1016/j.jhazmat.2017.07.044
14. Z. Chen, X. Yang, L. Song et al., Extraction and complexation of trivalent rare earth elements with tetraalkyl diglycolamides. Inorg. Chim. Acta **513**, 119928 (2020). https://doi.org/10.1016/j.ica.2020.119928
15. X.F. Yang, F.F. Li, P. Ren et al., Selective separation between UO_2^{2+} and Pu^{4+} by novel tetradentate chelate phenanthroline diamide ligand in 1-octanol. Sep. Purif. Technol. **277**, 119521 (2021). https://doi.org/10.1016/j.seppur.2021.119521
16. Y. Sugo, Y. Sasaki, S. Tachimori, Studies on hydrolysis and radiolysis of N, N, N', N'-tetraoctyl-3-oxapentane-1,5-diamide. Radiochim. Acta **90**, 161–165 (2002). https://doi.org/10.1524/ract.2002.90.3_2002.161
17. Y. Chen, S. Ning, Y. Zhong et al., Study on highly efficient separation of zirconium from scandium with TODGA-modified macroporous silica-polymer based resin. Sep. Purif. Technol. **305**, 122499 (2023). https://doi.org/10.2139/ssrn.4221764
18. M. Chen, Z. Li, Y. Geng et al., Adsorption behavior of thorium on N, N, N', N'-tetraoctyldiglycolamide (TODGA) impregnated graphene aerogel. Talanta **181**, 311–317 (2018). https://doi.org/10.1016/j.talanta.2018.01.020
19. J. Brown, F. Mclachlan, M. Sarsfield et al., Plutonium loading of prospective grouped actinide extraction (GANEX) solvent systems based on diglycolamide extractants. Solvent Extr. Ion Exch. **30**, 127–141 (2012). https://doi.org/10.1080/07366299.2011.609378
20. H. Yun-Ping, W. Jian, L. Can et al., Radiolytic stability of N-donor soft ligands for actinide(III)/lanthanide(III) separation. J. Nucl. Radiochem. **46**, 149–157 (2024). https://doi.org/10.7538/hhx.2024.YX.2023009
21. Z. Wang, L. Huang, X. Dong et al., Ion sieving in graphene oxide membrane enables efficient actinides/lanthanides separation. Nat. Commun. **14**, 261 (2023). https://doi.org/10.1038/s41467-023-35942-1
22. G. Modolo, A. Wilden, P. Kaufholz et al., Development and demonstration of innovative partitioning processes (i-SANEX and

1-cycle SANEX) for actinide partitioning. Prog. Nucl. Energy **72**, 107–114 (2014). https://doi.org/10.1016/j.pnucene.2013.07.021
23. S.L. Zhang, L. Yu, Y. Liu et al., Synthesis and study of bistriazolyl-pyrazines as new ligands for An/Ln separations. Sep. Purif. Technol. **357**, 130011 (2025). https://doi.org/10.2139/ssrn.4911242
24. Z.R. Ye, Q.Y. Wu, C.Z. Wang et al., Theoretical insights into the selective separation of Am(III)/Eu(III) using hydrophilic triazolyl-based ligands. Inorg. Chem. **61**, 6110–6119 (2022). https://doi.org/10.1021/acs.inorgchem.2c00232
25. W. Yuan, C. Wang, Y. Ao et al., γ-Radiation effect on Th^{4+} extraction behaviour of TODGA/[C_2mim][NTf_2]: identification and extractability study of radiolytic products. RSC Adv. **6**, 7626–7632 (2016). https://doi.org/10.1039/c5ra25364k
26. J. Ravi, T. Prathibha, K.A. Venkatesan et al., Third phase formation of neodymium(III) and nitric acid in unsymmetrical N, N-di-2-ethylhexyl-N'. N'-dioctyldiglycolamide. Sep. Purif. Technol. **85**, 96–100 (2012). https://doi.org/10.1016/j.seppur.2011.09.053
27. R.B. Gujar, S.A. Ansari, A. Bhattacharyya et al., Radiolytic stability of N, N, N', N'-tetraoctyl diglycolamide(TODGA) in the presence of phase modifiers dissolved in n-dodecane. Solvent Extr. Ion Exch. **30**, 278–290 (2012). https://doi.org/10.1080/07366299.2011.609389
28. H. Zhang, Y.Y. Ao, Y. Wang et al., Effect of radiolysis of TODGA on the extraction of TODGA/n-dodecane toward Eu(III): an experimental and DFT study. Nucl. Sci. Tech. **34**, 48 (2023). https://doi.org/10.1007/s41365-023-01198-z
29. H. Galán, A. Núñez, A.G. Espartero et al., Radiolytic stability of TODGA: characterization of degraded samples under different experimental conditions. Procedia. Chem. **7**, 195–201 (2012). https://doi.org/10.1016/j.proche.2012.10.033
30. Y.V. Nikitina, N.V. Yudin, E.V. Belova et al., The effect of aliphatic alcohol additives on the radiolytic degradation of TODGA in Isopar-M. J. Radioanal. Nucl. Chem. **326**, 1185–1192 (2020). https://doi.org/10.1007/s10967-020-07375-3
31. Y.V. Serenko, A.V. Ponomarev, E.V. Belova et al., Contribution of nitric acid and alcohol to the radiolytic degradation of TODGA in Isopar-M. J. Radioanal. Nucl. Chem. **328**, 1319–1328 (2021). https://doi.org/10.1007/s10967-021-07732-w
32. Q. Chen, C. Lu, Y. Hu et al., Extraction behavior of several lanthanides from nitric acid with DMDODGA in [C_4mim][NTf_2] ionic liquid. J. Radioanal. Nucl. Chem. **327**, 565–573 (2021). https://doi.org/10.1007/s10967-020-07525-7
33. Z. Dong, W.J. Yuan, C. Liu et al., Th(IV) and U(VI) removal by TODGA in ionic liquids: extraction behavior and mechanism, and radiation effect. Nucl. Sci. Tech. **28**, 62 (2017). https://doi.org/10.1007/s41365-017-0214-y
34. P. Zsabka, K. Van Hecke, A. Wilden et al., Gamma radiolysis of TODGA and $CyMe_4$BTPhen in the ionic liquid tri-n-octylmethylammonium nitrate. Solvent Extr. Ion Exch. **38**, 212–235 (2020). https://doi.org/10.1080/07366299.2019.1710918
35. Y. Dai, Y. Li, W. Hu et al., Functionalized ionic liquids based on DODGA with enhanced Eu(III)/U(VI) separation efficiency in highly acidic environment. J. Mol. Liq. **387**, 122557 (2023). https://doi.org/10.1016/j.molliq.2023.122557
36. A. Kimberlin, D. Guillaumont, S. Arpigny et al., An experimental and computational look at the radiolytic degradation of TODGA and the effect on metal complexation. New J. Chem. **45**, 12479–12493 (2021). https://doi.org/10.1039/d1nj01143j
37. D. Whittaker, M. Sarsfield, R. Taylor et al., Process flowsheet test of the i-SANEX process with CHON-compliant ligands in aqueous and organic phases. Prog. Nucl. Energy **166**, 104956 (2023). https://doi.org/10.1016/j.pnucene.2023.104956
38. A. Wilden, G. Modolo, P. Kaufholz et al., Laboratory-scale counter-current centrifugal contactor demonstration of an innovative-SANEX process using a water soluble BTP. Solvent Extr. Ion Exch. **33**, 91–108 (2015). https://doi.org/10.1080/07366299.2014.952532
39. A. Geist, U. Müllich, D. Magnusson et al., Actinide(III)/Lanthanide(III) separation via selective aqueous complexation of actinides(III) using a hydrophilic 2,6-bis(1,2,4-triazin-3-yl)-pyridine in nitric acid. Solvent Extr. Ion Exch. **30**, 433–444 (2012). https://doi.org/10.1080/07366299.2012.671111
40. D. Whittaker, A. Geist, G. Modolo et al., Applications of diglycolamide based solvent extraction processes in spent nuclear fuel reprocessing, part 1: TODGA. Solvent Extr. Ion Exch. **36**, 223–256 (2018). https://doi.org/10.1080/07366299.2018.1464269
41. M. Carrott, A. Geist, X. Heres et al., Distribution of plutonium, americium and interfering fission products between nitric acid and a mixed organic phase of TODGA and DMDOHEMA in kerosene, and implications for the design of the "EURO-GANEX'' process. Hydrometallurgy **152**, 139–148 (2015). https://doi.org/10.1016/j.hydromet.2014.12.019
42. M.J. Carrot, C.R. Gregson, R.J. Taylor, Neptunium extraction and stability in the GANEX solvent: 0.2 M TODGA/0.5 M DMDOHEMA/kerosene. Solv. Extr. Ion Exch. **31**, 463–482 (2013). https://doi.org/10.1080/07366299.2012.735559
43. M. Simonnet, L. Muller, T. Sittel et al., First investigations on a CHON UNEX process. Radiochim. Acta **111**, 597–600 (2023). https://doi.org/10.1515/ract-2023-0151
44. G. Modolo, H. Asp, C. Schreinemachers et al., Development of a TODGA based process for partitioning of actinides from a PUREX raffinate part I: batch extraction optimization studies and stability tests. Solv. Extr. Ion Exch. **25**, 703–721 (2007). https://doi.org/10.1080/07366290701634578
45. P. Deepika, K.N. Sabharwal, T.G. Srinivasan et al., Studies on the use of N, N, N', N'-tetra(2-ethylhexyl) diglycolamide (TEHDGA) for actinide partitioning II: investigation on radiolytic stability. Solv. Extr. Ion Exch. **29**, 230–246 (2011). https://doi.org/10.1080/07366299.2011.539145
46. S.Y. Nong, J.W. Zheng, S.Y. Yang et al., Gamma radiation decomposition and the extraction performance of TODGA in kerosene medium. Nucl. Tech. **47**, 060303 (2024). https://doi.org/10.11889/j.0253-3219.2024.hjs.47.060303. (**in Chinese**)
47. C. Lee, W. Yang, R.G. Parr, Development of the Colle-Salvetti correlation-energy formula into a functional of the electron density. Phys. Rev. B **37**, 785 (1988). https://doi.org/10.1103/physrevb.37.785
48. W. Xu, Y. Zhou, D. Huang et al., Luminescent sensing profiles based on anion-responsive lanthanide (III) quinolinecarboxylate materials: solid-state structures, photophysical properties, and anionic species recognition. J. Mater. Chem. C **3**, 2003–2015 (2015). https://doi.org/10.1039/c4tc02369b
49. A.D. Beck, Density-functional thermochemistry. III. the role of exact exchange. J. Chem. Phys. **98**, 5648–5652 (1993). https://doi.org/10.1063/1.464913
50. R. Dennington, T. Keith, J. Millam et al., GaussView, Version 6.1.1. Shawnee Mission, KS (2019). https://gaussian.com/gv611rn/
51. Y.L. Wang, F.F. Li, Z. Xiao et al., Experimental and theoretical studies on the extraction behavior of Cf(III) by NTAamide(C8) ligand and the separation of Cf(III)/Cm(III). RSC Adv. **13**, 3781–3791 (2023). https://doi.org/10.1039/d2ra07660h
52. Q. Wu, H. Hao, Y. Liu et al., Selective separation of americium(III), curium(III), and lanthanide(III) by aqueous and organic competitive extraction. Inorg. Chem. **63**, 462–473 (2023). https://doi.org/10.1021/acs.inorgchem.3c03331
53. T. Lu, F. Chen, Multiwfn: a multifunctional wavefunction analyzer. J. Comput. Chem. **33**, 580–592 (2012). https://doi.org/10.1002/jcc.22885

54. J. Zhang, T. Lu, Efficient evaluation of electrostatic potential with computerized optimized code. Phys. Chem. Chem. Phys. **23**, 20323–20328 (2021). https://doi.org/10.1039/d1cp02805g
55. T. Lu, A comprehensive electron wavefunction analysis toolbox for chemists. Multiwfn. J. Chem. Phys. **161**, 082503 (2024). https://doi.org/10.1063/5.0216272
56. W. Humphrey, A. Dalke, K. Schulten, VMD: visual molecular dynamics. J. Mol. Graph. **14**, 33–38 (1996). https://doi.org/10.1016/0263-7855(96)00018-5
57. B.J. Mincher, G. Modolo, S.P. Mezyk, Review article: The effects of radiation chemistry on solvent extraction: 1. Conditions in acidic solution and a review of TBP radiolysis. Solv. Extr. Ion Exch. **27**, 1–25 (2009). https://doi.org/10.1080/07366290802544767
58. C.A. Zarzana, G.S. Groenewold, B.J. Mincher et al., A comparison of the γ-radiolysis of TODGA and T(EH)DGA using UHPLC-ESI-MS analysis. Solv. Extr. Ion Exch. **33**, 431–447 (2015). https://doi.org/10.1080/07366299.2015.1012885
59. D.D. Dicholkar, P. Kumar, P.K. Heer et al., Synthesis of N, N, N', N'-tetraoctyl-3-oxapentane-1,5-diamide (TODGA) and its steam thermolysis-nitrolysis as a nuclear waste solvent minimization method. Ind. Eng. Chem. Res. **52**, 2457–2469 (2013). https://doi.org/10.1021/ie302603q
60. B. Verlinden, K. Van Hecke, A. Wilden et al., Gamma radiolytic stability of the novel modified diglycolamide 2,2'-oxybis(N, N-didecylpropanamide) (mTDDGA) for grouped actinide extraction. RSC Adv. **12**, 12416–12426 (2022). https://doi.org/10.1039/d1ra08761d
61. Y. Sasaki, Y. Sugo, Y. Kitatsuji et al., Complexation and back extraction of various metals by water-soluble diglycolamide. Anal. Sci. **23**, 727–731 (2007). https://doi.org/10.2116/analsci.23.727
62. A. Wilden, G. Modolo, S. Lange et al., Modified diglycolamides for the An(III) + Ln(III) co-separation: evaluation by solvent extraction and time-resolved laser fluorescence spectroscopy. Solv. Extr. Ion Exch. **32**, 119–137 (2014). https://doi.org/10.1080/07366299.2013.833791
63. A. Sengupta, P.K. Mohapatra, M. Iqbal et al., Spectroscopic investigations of Eu^{3+}-complexes with ligands containing multiple diglycolamide pendant arms in a room temperature ionic liquid. J. Lumines. **154**, 392–401 (2014). https://doi.org/10.1016/j.jlumin.2014.05.001
64. P.N. Pathak, S.A. Ansari, S.V. Godbole et al., Interaction of Eu^{3+} with N, N, N', N'-tetraoctyl diglycolamide: A time resolved luminescence spectroscopy study. Spectroc. Acta Pt. A-Molec. Biomolec. Spectr. **73**, 348–352 (2009). https://doi.org/10.1016/j.saa.2009.02.040
65. T. Sun, F. Huang, J. Liu et al., Strengthened d-p orbital-hybridization of single atoms with sulfur species induced bidirectional catalysis for lithium–sulfur batteries. Adv. Funct. Mater. **33**, 2306049 (2023). https://doi.org/10.1002/adfm.202306049
66. L. Xu, X.K. Zhao, H. Cao et al., Complexation of hexavalent neptunium(VI) with oxydiacetic acid and its amide derivatives in aqueous solution: Spectrophotometry and DFT calculations. Inorg. Chem. **63**, 6173–6183 (2024). https://doi.org/10.1021/acs.inorgchem.3c04221
67. G. Yu, L. Lyu, F. Zhang et al., Theoretical and experimental evidence for rGO-4-PP Nc as a metal-free Fenton-like catalyst by tuning the electron distribution. RSC Adv. **8**, 3312–3320 (2018). https://doi.org/10.1039/c7ra12573a
68. X.H. Kong, Q.Y. Wu, J.H. Lan et al., Theoretical insights into preorganized pyridylpyrazole-based ligands toward the separation of Am(III)/Eu(III). Inorg. Chem. **57**, 14810–14820 (2018). https://doi.org/10.1021/acs.inorgchem.8b02550